EAI Endorsed Transactions
on Digital Transformation on Industrial Processes Research Article EAI.EU

Experimental Investigation of Localised Laser Heat Treatment Effects on 6XXX Aluminium Alloys: Critical Insights into Numerical Modelling

M. Fernandes[1, 2*], S. Teixeira[1] and N. Peixinho[2]

[1] Centro ALGORITMI/LASI, University of Minho, 4800-058 Guimarães, Portugal
[2] Centro MEtRICs, University of Minho, 4800-058 Guimarães, Portugal

Abstract

To meet global emission reduction targets, high specific strength materials, such as 6XXX-series aluminium alloys, are integrated into automotive structures. Although self-piercing riveting (SPR) is a highly adopted joining technique in the referred industry, the low cold formability of these alloys can lead to failure in the sheet material. Thus, a promising solution is the application of a localised laser heat treatment that will promote the local softening of the material and, therefore, prevent its failure.
A prior numerical study introduced localised laser heat treatment to solve the bottom sheet failure problem but simplified it by assuming homogeneous hardness throughout the treated thickness and strict confinement of the softened zone. However, these simplifying assumptions lack rigorous experimental validation. To address this gap, this work aims to assess the validity of these simplifications. For this purpose, an experimental analysis was conducted on four samples of AA6063-T6 subjected to a localised laser heat treatment applied to an annular region defined by internal and external diameters of 4 and 7.5 mm. The resulting hardness profiles were subsequently analysed. Results demonstrate that the laser-induced softening was not confined to the intended annular region and did not occur uniformly through the sheet thickness. These findings reveal discrepancies between the real softening behaviour and the assumptions adopted in the numerical model.

Keywords: Industrial Processes, 6063-T6 Aluminium Alloy, Localised Laser Heat Treatment, Hardness Profile, Experimental Study, Self-Piercing Riveting.

Received on 18 December 2025, accepted on 13 February 2026, published on 19 February 2026

doi: 10.4108/dtip.11402

1. Introduction

According to provisional data from the European Environment Agency (EEA) [1], in 2024 Europe saw an increase in emitted CO_2/km of 4.5 g/km compared to 2023, after a significant reduction from 2020 to 2023. The transport industry is responsible for the largest CO_2 emissions, with passenger cars and light commercial vehicles representing around 16% and 3%, respectively [2]. Following this, the reduction in fossil fuel consumption can be achieved by reducing the weight of automobiles. To this end, materials with high specific strength, such as certain 6XXX-series aluminium alloys and high-strength steels, are adopted, without neglecting passenger safety in the event of a collision [3–5]. Recent studies on Al6061 have demonstrated that the optimization of microstructural properties through T6 heat treatment is fundamental to achieve superior mechanical performance, especially when considering reinforced matrix composites [6]. In fact, the control of precipitation hardening through specific ageing cycles, such as T6 and T8, has been

*Corresponding author. Email: d14919@dem.uminho.pt

shown to significantly influence the mechanical response and fracture modes of high-strength aluminium systems, allowing for a more precise tailoring of material properties [7].While the use of these materials is crucial for lightweighting, their integration poses significant challenges for joining processes. Conventional methods such as resistance spot welding are often unsuitable. Furthermore, welding dissimilar materials like Al and steel is challenging due to large melting point differences [8,9]. Consequently, joining processes based on plastic deformation are attractive, as they offer high productivity and low cost, and are applicable to multi-material design [9]. Self-Piercing Riveting (SPR) is one of the most widely adopted and advantageous mechanical joining processes in the automotive industry, particularly for body-in-white applications [10–11]. However, the SPR of these materials imposes limitations related to their low ductility, commonly leading to failure of the bottom sheet (the one in contact with the die). Thus, the application of localised heat treatments that enable material softening emerges as a possible solution [12,13].

Peixinho et al. [14] validated the effectiveness of applying localised laser heat treatments to achieve the required hardness reduction in 6XXX-series aluminium alloys, concluding that the process is a robust approach to locally manipulate properties. This softening is crucial for facilitating subsequent forming processes through stress redistribution. In line with this objective, Palmieri et al. [15] conducted a numerical study on optimizing softening strategies via localised laser heat treatment, also in 6XXX-series aluminium alloy sheets. The results showed the difficulty of obtaining a uniform hardness distribution through the sheet thickness due to the large thermal gradient observed, with pulsed heating being highlighted as effective. The experimental results validated the numerically predicted results. Expanding the application of this methodology to other metallic systems, Kim et al. [16] performed a localised laser heat treatment on 316L stainless steel to optimize its forming process. By inducing controlled surface austenitization, creating a more ductile surface layer while maintaining a resistant core (thermally unaffected), the authors successfully formed the steel while retaining its characteristic mechanical strength. Similarly, Graser et al. [17] experimentally demonstrated that the application of a localised heat treatment is capable of locally reducing hardness and increasing ductility of steel only in the joining zone, thereby preventing failures and cracks while maintaining the high mechanical properties of the remaining component.

Despite the evidence supporting laser-induced softening to improve formability of high specific strength materials, literature remains scarce regarding its direct application to optimize the SPR process in 6XXX-series alloys. To address this, Fernandes et al. [12] developed a 3D numerical model that incorporated Johnson-Cook constitutive equations to define the material flow and introduced the concept of localized softening to mitigate bottom sheet failure. However, this model assumed an idealized 34 % hardness reduction within a strictly confined annular zone (4 – 7.5 mm) with perfect through-thickness homogeneity—premises that lack rigorous experimental validation. Given this, the present work contributes by experimentally assessing the validity of the aforementioned assumptions through a critical analysis of hardness profiles in 6063-T6 samples. By identifying the discrepancies between idealised numerical softening and actual thermal-mechanical behaviour, this study provides the empirical data necessary to calibrate and update the numerical model, enabling more accurate predictions of the final strength of the SPR joint.

2. Materials and Methods

Following the numerical work developed by Fernandes et al. [12], an experimental study was conducted to assess the influence of a localised laser heat treatment on the hardness of 6063-T6 aluminium alloy samples. This experimental analysis enables a direct comparison of the experimental results with the numerical predictions, providing a critical evaluation of the assumptions adopted in the numerical model. It is important to note that this alloy differs from the 6061-T6 used in the numerical model, however, the selection of the experimental material, 6063-T6, was dictated by its availability. Since both alloys exhibit broadly similar precipitation mechanisms, namely the dissolution of β'' precipitates upon heating [18], the comparison of the localised heat treatment effects is considered valid for evaluating the model's thermos-mechanical assumptions.

The overall experimental workflow is summarised in Figure 1.

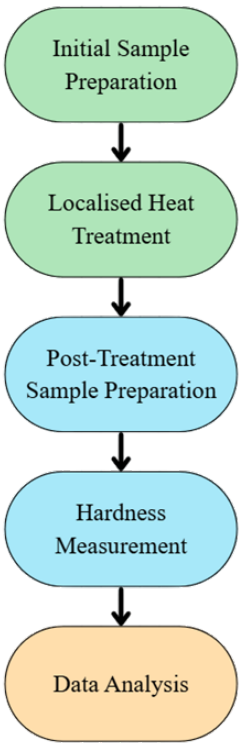

Figure 1. Experimental workflow summarising the main stages of the experimental study

2.1. Localised Laser Heat Treatment

In order to experimentally reproduce the assumptions considered in the numerical model, enabling a critical comparison between predicted and measured material behaviour, a localised laser heat treatment was applied to 6063-T6 aluminium alloy samples, in accordance with the parameters corresponding to the highest performance prediction.

Sample Preparation

The localised laser heat treatment was performed on 4 samples of 6063-T6 aluminium alloy, shown in Figure 2, given the material availability. These samples were obtained from a square section tube with a 2 mm thickness using an electric saw. Subsequently, they were cut to obtain the following final dimensions: 22×22×2 mm.

Figure 2. 6063-T6 aluminium alloy samples sourced from a square section tube

Aluminium alloys have a low energy absorption rate and, therefore, high reflectivity of lasers at room temperature, which leads to a reduction in the amount of energy absorbed, with consequences for the adequate penetration of the material to be heat treated [19]. Hence, in order to maximise the amount of laser energy absorbed by aluminium alloys, a thin layer of graphite should be applied to the surface [20,21].

Equipment and Experimental Procedure

After the proper preparation of the samples, the localised laser heat treatment was carried out using the LM100 Diode Laser provided by PIEP - Polymer Engineering Innovation Centre at the University of Minho. For this process, a maximum temperature of 420 ˚C and a feed rate of 1 mm/s were defined, with the heat treatment being applied to a ring-shaped area with inner and outer diameters of 4 and 7.5 mm, respectively.

In order to calibrate the focal length of the laser so that the area affected by it corresponded to the thickness of the ring (2.5 mm), a quadrangular cutout with a delimited central ring was used, as shown in Figure 3.

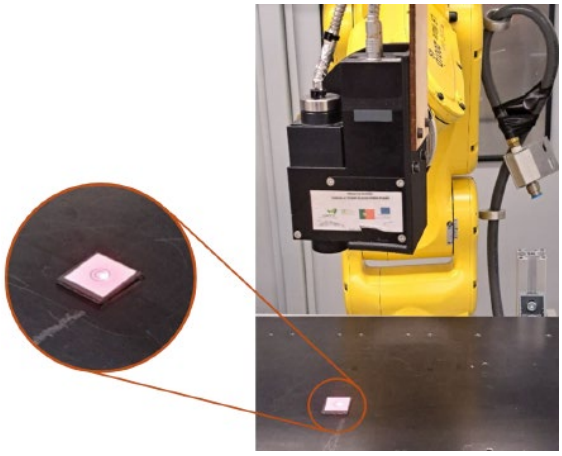

Figure 3. Initial process of calibrating the laser focal length using a paper cut-out with the central ring marked out

Once the setup was complete, the localised heat treatment was performed sequentially on the four samples, designated A1, A2, A3, and A4. The system's protocol was established such that the robotic arm was only activated once the laser reached the target temperature of 420 ºC. The time required for the heat treatment procedure, t_p,varied slightly between samples: for Sample A1, the process lasted approximately 70 s, while the remaining samples were completed in approximately 50 s.

Table 1 summarises the heating time t_h and the heat treatment procedure time t_p for each sample.

Table 1. Summary of the heating time, t_h, and the heat treatment procedure time, t_p, for each sample

Sample	t_h [s]	t_p [s]
A1	15	70
A2	9.5	50
A3	4	50
A4	8.5	50

2.2. Hardness Measurement

Once the heat treatment of each sample has been completed, the next step is to analyse their hardness in order to verify whether the objective has been achieved: softening of the heat-treated area.

Sample Preparation

Following the heat treatment and removal of the graphite coating (used as an absorption layer during the laser process), a cut was made in the centre of the samples, followed by sanding of the cut thickness on the rotating griding machine

in order to enable hardness analysis along that thickness. This initial sanding step ensures that all the samples are of equal height, facilitating their standardization for the subsequent stages of the procedure.

The samples were then placed in appropriate moulds (Figure 4 a), where a resin was poured to secure them and facilitate the measurement of hardness along the thickness (Figure 4 b). After the resin had cured (Figure 4 c), the surfaces to be measured were polished using a finer grit abrasive paper than the one previously used (Figure 4 d).

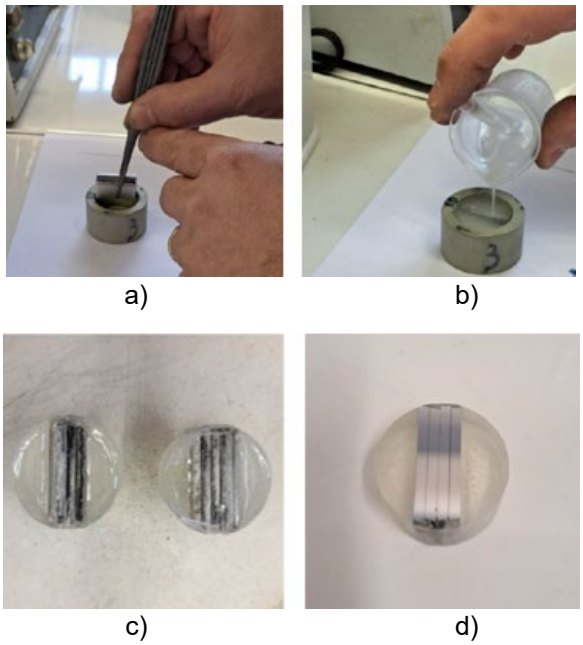

Figure 4. Experimental procedure: a) Positioning of samples in the mould; b) Addition of resin to the moulds containing the samples; c) Samples after resin curing; d) Polishing of the surface to be measured

Equipment and Measurement Procedure

Hardness tests were performed on the prepared samples using a Shimadzu Model 4451 hardness tester at an applied load of 50 gf and a dwell time of 15 s.

To assess the hardness of the samples, a sample that had not undergone any heat treatment, designated Sample BM (Base Material), was taken as a reference. From this sample, a single Vickers indentation was performed at each of the three distinct locations shown in Figure 5 (L1, L2, and L3), providing a representative average of the material's initial state. Position L1 was considered to be the origin, with positions L2 and L3 5 mm away from the origin position.

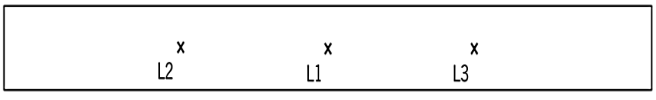

Figure 5. Diagram of the locations where hardness measurements were taken on the BM sample

Regarding Sample A1, hardness was measured according to the positions shown in the diagram presented in Figure 6. In this scheme, each indicated 'x' corresponds to a single Vickers indentation. The positions on the incidence surface have a uniform spacing of 2 mm between them, while the positions at the center of the thickness possess a uniform spacing of 5 mm. The central positions L1 and L2 are considered the reference origins. Also in the diagram, the zone theoretically affected by the heat treatment is marked in grey.

This initial measurement scheme was adopted as a pilot test to assess the necessary measurement density, leading to the subsequent adoption of an optimized scheme for the remaining samples.

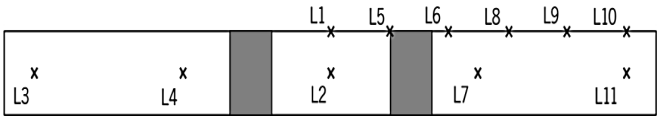

Figure 6. Diagram of the locations where hardness measurements were taken on the A1 sample

Thus, for Samples A2, A3, and A4, a new hardness measurement scheme was adopted, which is presented in Figure 7. Similarly, each location marked with an 'x' represents one individual reading, ensuring a uniform spacing of 5 mm at both the incidence surface and the center of the thickness. In the diagram, the regions marked in grey correspond to the heat treated zone.

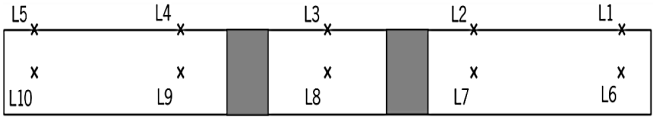

Figure 7. Diagram of the locations where hardness measurements were taken on A2, A3 and A4 samples

3. Results and Discussion

3.1 Localised Laser Heat Treatment Analysis

During the localised laser heat treatment procedure, the heating curves for samples A1, A2, A3, and A4 were recorded. The analysis of these curves allows for the evaluation of the thermal response of each sample as a function of the defined maximum temperature (420 ºC) and the associated procedure time, t_p.

The heating curves for all samples are detailed in the Appendix. For a better understanding, Figure 8 particularly

illustrates Sample's A1 heating curve. Here, the green and red curves characterize the target temperature (420 ºC) and the temperature reached by the laser, respectively. From the graph in Figure 9 it is clear that the laser reaches the target temperature after approximately 15 s and proceeds to heat treat the sample for about 70 s.

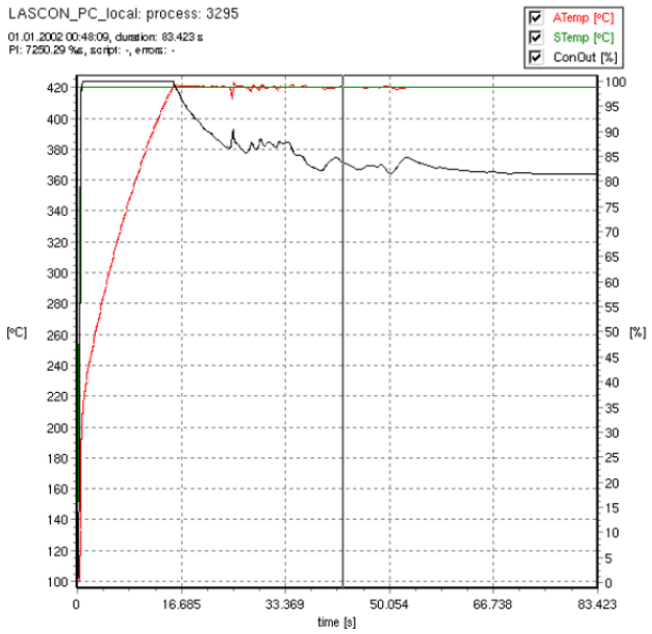

Figure 8. Sample A1 heating curve

3.2 Hardness Profile Evaluation

Base Material Characterization (BM Sample)

As previously mentioned, the BM (Base Material) sample that did not undergo any heat treatment was taken as a reference. Hardness was recorded at the positions presented in the diagram shown in Figure 5.

Table 2 comprises the measured hardness values for the three positions indicated in the diagram.

Table 2. Hardness values (HV) measured on the BM sample across three locations, according to Figure 5

Position	L1	L2	L3
Hardness [HV]	83	85	83

Based on the obtained results, a slight variation of 2.35 % is observed between the hardness values of positions L2 and L1, which suggests a relatively homogeneous hardness throughout the sample. With values concentrated around 84 HV and a standard deviation of 1 HV, the results demonstrate the homogeneity of the base material. These homogeneity results are detailed and visually illustrated in Figure 9.

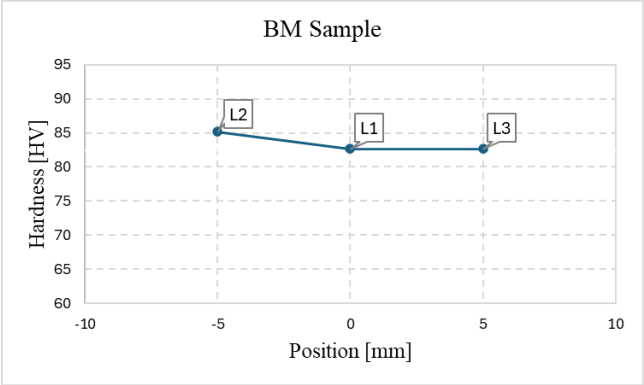

Figure 9. Hardness profile variation of the Base Material (BM) sample along the measured thickness positions

Hardness Profile of Heat Treated Samples

Following the confirmation of base material homogeneity, this section presents the Vickers hardness profiles measured across the heat-treated samples (A1 to A4), detailing the effect of the localised laser heat treatment. Thus, regarding Sample A1, the measured hardness values, according to the positions shown in the diagram in Figure 6 are summarized in Table 3.

Table 3. Hardness values (HV) measured across sample A1, according to Figure 6

Position	Hardness [HV]
L1	58
L2	58
L3	64
L4	58
L5	58
L6	64
L7	66
L8	66
L9	70
L10	72
L11	66

Based on the obtained data, a global reduction in the sample's hardness is observed, which presents average values lower than those of the BM Sample. This considerable decrease in hardness can be attributed to the total time of exposure to the heat treatment 15 s of heating and 70 s of treatment at a temperature of 420 ºC.

Pertaining to the hardness values evaluated on the incidence surface, a significant reduction in hardness is observed at positions L1 and L5, corresponding to the interior of the heat treated ring, with a hardness of 58 HV. As the distance from the heat treated zone increases, there is a gradual increase in hardness, rising to 72 HV at L10, which indicates that outside the treated region, the sample maintains

a higher hardness. Thus, the heat treatment produced a localised softening of 24 % on the incidence surface. At the center of the sample's thickness, the hardness is 58 HV at both L2 and L4, suggesting that the heat treatment was also capable of softening the central region. Similarly, outside the TT region, the hardness increases to higher levels, ranging between 64 HV and 66 HV. Thus, the heat treatment led to a localised softening of 13.8 % at the center of the sample.
Quantitatively, the numerical model [12] predicts a target hardness of 55 HV (representing a 34% reduction from the 84 HV baseline). Although the experimental results for Sample A1 show values as low as 58 HV, with a numerical deviation of only 5.4%, validating the softening magnitude, this effect was not restricted to the annular heat treated area.

These results are detailed and visually illustrated in Figure 10.

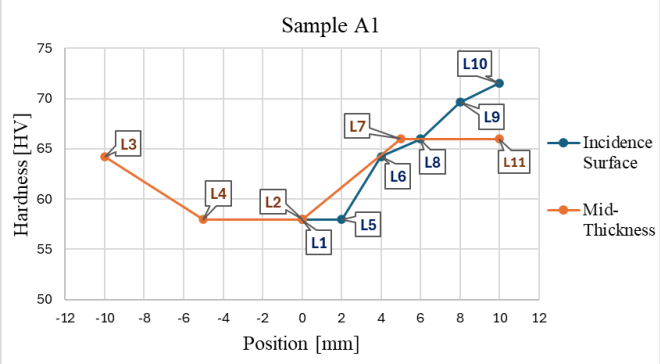

Figure 10. Hardness profile variation of sample A1

As previously detailed, an optimized hardness measurement scheme was adopted for samples A2, A3, and A4, as presented in Figure 8. The measured hardness values for the marked positions on these three samples are comprehensively summarized in Table 4.

Table 4. Hardness values (HV) measured across samples A2, A3 and A4, according to Figure 7

Position [mm]	Hardness [HV]		
	Sample A2	Sample A3	Sample A4
L1	70	80	64
L2	68	83	58
L3	68	78	63
L4	72	76	58
L5	78	80	66
L6	72	76	66
L7	72	70	64
L8	64	83	61
L9	68	78	64
L10	72	78	66

Focusing initially on sample A2, results confirm that the heat treatment promoted an overall reduction in the sample's hardness. Specifically, on the incidence surface, an expressive reduction to 68 HV is observed at L3, the position corresponding to the center of the heat treated ring. Outside the treated zone, the hardness values show a greater variation for the positions to the left of the origin, suggesting lateral thermal diffusion beyond the defined ring area. Thus, the heat treatment produced a softening of 12.8 % at L3.

Along the centre of the sample's thickness, a decrease in hardness is observed to the left of the origin, suggesting that these positions were affected by the heat treatment; however, this is not verified to the right of the origin. A hardness reduction of 12.5 % is noted at the center of the heat treated ring, corresponding to position L8. Although the localized softening effect remains 16.3 % above the numerical target of 55 HV, the non-symmetrical softening and the varying degrees of reduction between the surface and the center of the thickness indicate that the hardness change is not uniform through the sample's depth. This finding highlights the sensitivity of the 6063-T6 aluminium alloy to the thermal cycle parameter.

These results are detailed and visually illustrated in Figure 11.

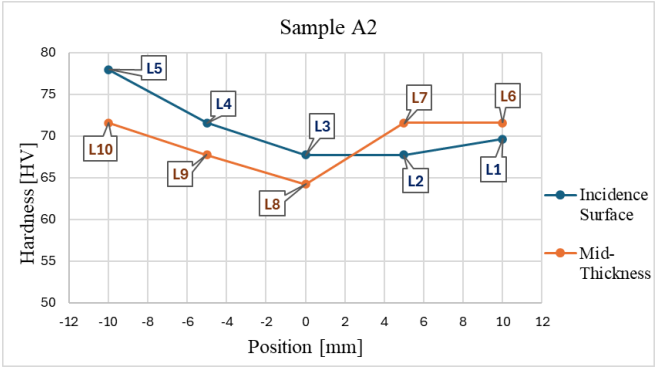

Figure 11. Hardness profile variation of sample A2

Conversely, for sample A3 the heat treatment did not yield the expected effect—the localised softening of the sample — since the hardness values remain notably high without significant evidence of reduction, as clearly illustrated in Figure 12. Observing the profiles, the hardness values across the incidence surface (blue line) remain concentrated between 77 HV and 83 HV, which is close to the initial Base Material hardness of 84 HV. This failure to achieve the desired softening can be attributed to the low energy absorption peak observed during the procedure, resulting from the inefficient application of the graphite coating.

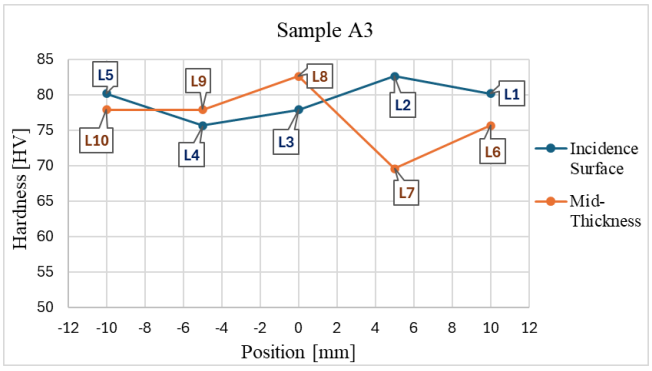

Figure 12. Hardness profile variation of sample A3

Finally, regarding sample A4, Figure 13 shows that, similar to samples A1 and A2, the heat treatment promoted an overall reduction in the sample's hardness.

Concerning the hardness values on the incidence surface, a greater hardness reduction is verified outside the treated ring at L2 and L4 (58 HV), rather than at its centre, as occurred in the previous samples. This minimum value of 58 HV represents a significant correlation with the 55 HV target predicted by the numerical model [12], showing a deviation of only 5.4 %. This asymmetrical profile suggests that the effective heating center of the laser may have been slightly off-centre relative to the marking, or that lateral heat diffusion was dominant. In the region external to the thermally affected ring, a significant softening of 12.2 % is measured.

At the center of the sample's thickness, a localised softening of 7.6 % is observed at the centre of the heat treated ring. With the distance from the reference origin, the hardness assumes higher values. When compared numerically, the 7.6 % softening at the mid-thickness is considerably lower than the 34 % reduction assumed in the numerical model [12], reinforcing that the assumption of through-thickness homogeneity is not experimentally verified.

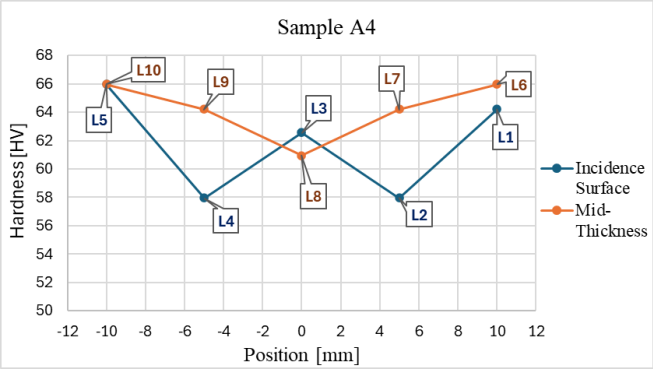

Figure 13. Hardness profile variation of sample A4.

4. Conclusions

The present study focused on the empirical assessment of the numerical premises for localized laser softening in AA6063-T6 alloys used for SPR joints assumed in the work of Fernandes et al. [12]. The specific inferences drawn from these investigations are summarized as follows:

- The AA6063-T6 base material exhibited a stable hardness of 84 ± 1 HV. Samples A1 and A4 reached minimum values of 58 HV, showing a high correlation with the numerical target of 55 HV (a 5.4 % deviation).
- The heat treatment exceeded the intended annular zone (4 – 7.5 mm) due to lateral thermal diffusion. Furthermore, the lack of softening in Sample A3 (77–83 HV) highlights the critical role of energy absorption efficiency in industrial laser.
- Contrary to the numerical assumption of a strictly confined and through-thickness homogeneous zone, experimental profiles revealed significant gradients, with softening levels varying between 24% on the surface and 13.8% at mid-thickness in Sample A1.
- A generalized reduction in the overall hardness of all samples (except Sample A3) was observed when compared to the base material, reflecting the predominant influence of exposure time and thermal intensity of the treatment.
- In certain cases, the localised hardness reduction near the incidence surface proved to be non-uniform, raising crucial questions regarding the confinement and hardness distribution assumptions of the numerical model.
- Results show that the premises of the numerical model are partially invalidated. The numerical model, by assuming these ideal uniform softening conditions, overestimates the effective softening in the sheet, which may lead to inaccurate prediction of the final strength of the resulting SPR joint.

Given this, results emphasize the need for strict control of heat-treatment parameters to balance the desired effects of localised softening and structural preservation. One possible solution would be the implementation of a laser beam shaped as a ring, thereby avoiding the circular motion currently used to form the ring and, in turn, restricting thermal effects exclusively to the intended zone.

Thus, these results establish the basis for calibrating the existing numerical model. Future work should focus on updating the simulations—either by incorporating experimental data or through coupled thermal-structural analyses—followed by SPR tests to validate the predicted joint strength against experimental findings. Finally, considering the industrial relevance of these findings, the scalability of localized laser softening depends on its integration into high-volume production environments. While laser technology is already a staple in automotive manufacturing, establishing robust industrial parameter windows is paramount to ensure process repeatability. Addressing the sensitivity of the softening effect to manufacturing tolerances will be a decisive step in

transitioning this methodology from a laboratory-proven concept to a viable industrial solution.

Appendix – Heating Curves

The following figures provide the complete set of localised heat treatment temperature profiles for the samples not illustrated in the main text, specifically A2, A3, and A4 (see Figures A.1, A.2, A.3, respectively).

Distinctly, for Sample A3 (Figure A.2), it is seen that the laser reaches the target temperature after 4 s. Nevertheless, in the time interval between 33.3 s and 41.8 s, a notable low absorption peak is observed during the procedure phase. This anomaly can be attributed to an inefficient application of the graphite layer on the sample's incidence surface.

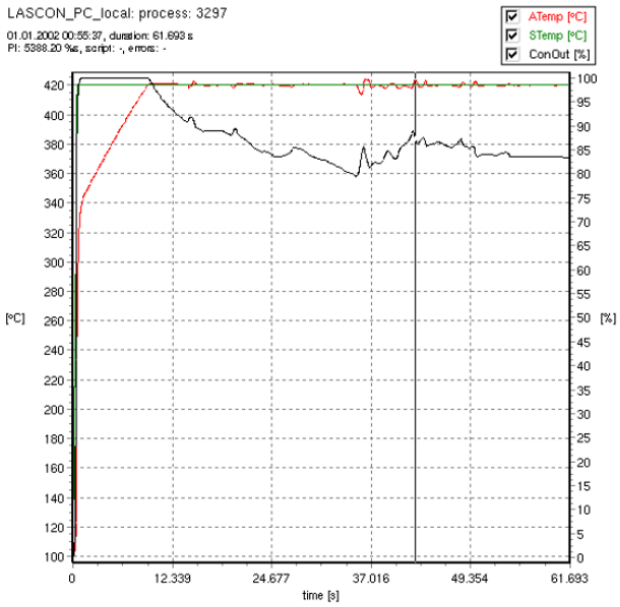

Figure A.1. Sample A2 heating curve

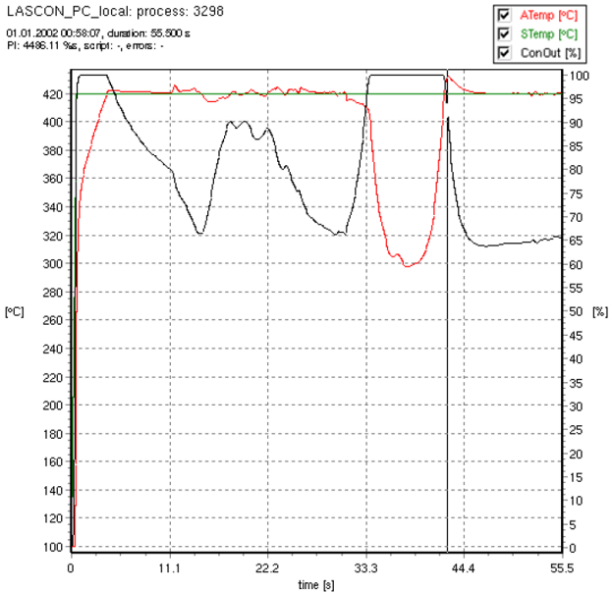

Figure A.2. Sample A3 heating curve

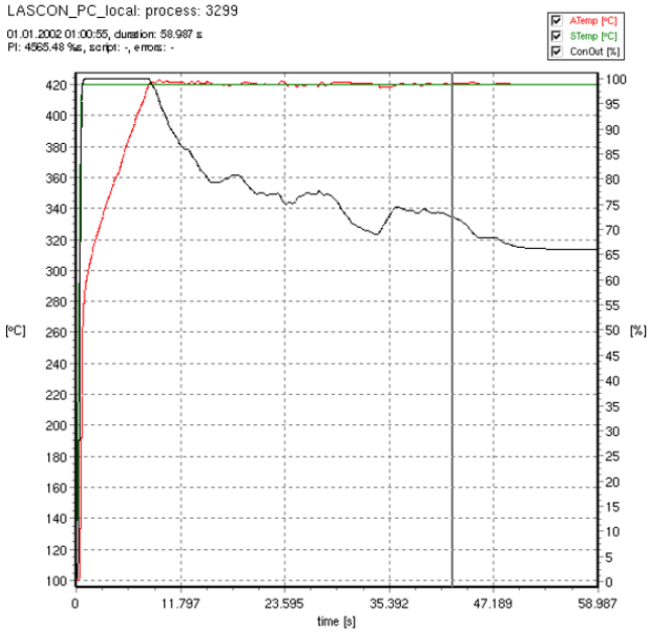

Figure A.3. Sample A4 heating curve

Acknowledgements.

This work was supported by PIEP – Polymer Engineering Innovation Centre, I.P. by project scope UIBD/EMS/04077/2020 (MEtRICs) and by project scope UID/CEC/00319/2020 (ALGORITMI).

References

[1] European Environment Agency. Average CO2 emissions from new cars and new vans slightly increased in 2024 [Internet]. 2025. Available from:

https://www.eea.europa.eu/en/newsroom/news/average-co2-emissions-from-new-cars-and-new-vans.
[2] Institutional Investors Group on Climate Change. Policy briefing: EU CO2 emission performance standards for new passenger cars and vans. 2025.
[3] Mori K ichiro, Abe Y. A review on mechanical joining of aluminium and high strength steel sheets by plastic deformation. International Journal of Lightweight Materials and Manufacture. 2018 Mar;1(1):1–11.
[4] Rajalingam P, Rajakumar S, Sonar T, Kavitha S. A comparative study on resistance spot and laser beam spot welding of ultra-high strength steel for automotive applications. International Journal of Lightweight Materials and Manufacture. 2024 Sep;7(5):648–61.
[5] Zhu L, Li N, Childs PRN. Light-weighting in aerospace component and system design. Propulsion and Power Research. 2018 Jun;7(2):103–19.
[6] P B, M AX. Effect of B4C and graphene on the microstructural and mechanical properties of Al6061 matrix composites. Journal of Materials Research and Technology. 2024 Jul;31:496–505.
[7] Parasuraman B, Pazhani A, Michael AX, Pitchaimuthu S, Batako A. Effect of T6 and T8 Ageing on the Mechanical and Microstructural Properties of Graphene-Reinforced AA2219 Composites for Hydrogen Storage Tank Inner Liner Applications. Journal of Composites Science. 2025 Jun 25;9(7):328.
[8] Barnes TA, Pashby IR. Joining techniques for aluminium spaceframes used in automobiles. J Mater Process Technol. 2000 Mar;99(1–3):72–9.
[9] Mori K ichiro, Abe Y. A review on mechanical joining of aluminium and high strength steel sheets by plastic deformation. International Journal of Lightweight Materials and Manufacture. 2018 Mar;1(1):1–11.
[10] Sankaranarayanan R, Hynes NRJ, Nikolova MP, Królczyk JB. Self-Pierce Riveting: Development and Assessment for Joining Polymer—Metal Hybrid Structures in Lightweight Automotive Applications. Polymers (Basel). 2023 Oct 11;15(20):4053.
[11] Wang C, Du Z, Cheng A, He Z, Tan H, Yu W. Influence of process parameters and heat treatment on self-piercing riveting of high-strength steel and die-casting aluminium. Journal of Materials Research and Technology. 2023 Sep;26:8857–78.
[12] Fernandes M, Peixinho N. Improvement of Multi-material Joining Techniques Via Localised Heat Treatment. In: Machado J, Trojanowska J, Ottaviano E, Xavior MA, Valášek P, Basova Y, editors. Innovations in Mechanical Engineering IV. Springer; 2025. p. 65–76.
[13] Pereira R, Peixinho N, Carneiro V, Soares D, Cortez S, Costa SL, et al. An Experimental and Numerical Study on Aluminum Alloy Tailor Heat Treated Blanks. Journal of Manufacturing and Materials Processing. 2023 Jan 4;7(1):16.
[14] Peixinho N, Pereira R, Carneiro V, Cortez S, Costa S, Blanco V. Development of Laser Heat Treatment Process for Assisted Forming of Aluminum Alloys. International Journal for Engineering Modelling. 2023 Dec 20;37(1).
[15] Palmieri ME, Tricarico L. Investigation of Two Laser Heat Treatment Strategies for Local Softening of a Sheet in Age-Hardening Aluminum Alloy by Means of Physical Simulation. J Mater Eng Perform. 2024 Sep 9;33(18):9612–25.
[16] Kim RE, Gu GH, Lee JA, Choi YT, Park H, Kim J, et al. Surface heterostructuring in laser-treated alloys through local austenitization for high strength and formability. Mater Res Lett. 2024 Aug 2;12(8):606–15.
[17] Graser M, Wiesenmayer S, Müller M, Merklein M. Application of Tailor Heat Treated Blanks technology in a joining by forming process. J Mater Process Technol. 2019 Feb;264:259–72.
[18] Vogl LM, Schweizer P, Donohue J, Minor AM. Correlated 4D-STEM and EDS for the classification of fine Beta-precipitates in aluminum alloy AA 6063-T6. Scr Mater. 2024 Dec;253:116288.
[19] Hassel T, Beniyash A, Klimov G. Non-vacuum electron beam welding and cutting of cupper. IOP Conf Ser Mater Sci Eng. 2020 Feb 1;759(1):012003.
[20] Man HC, Zhang S, Cheng FT. Improving the wear resistance of AA 6061 by laser surface alloying with NiTi. Mater Lett. 2007 Aug;61(19–20):4058–61.
[21] Romme C. Aluminium [Internet]. 2025. Available from: https://abc-vietnam.com/laser-cutting-aluminum/#:~:text=Aluminum%20exhibits%20high%20reflectivity%20for%20infrared%20wavelengths%2C,the%20energy%20is%20reflected%20rather%20than%20absorbed.